Fabrication techniques for creating a thermally isolated TM-FPA (thermal microphotonic focal plane array)

Michael J. Shaw, Michael R. Watts, Gregory N. Nielson

Sandia National Laboratory, P.O. Box 5800, Albuquerque New Mexico 87185
mjshaw@sandia.gov

ABSTRACT

A novel fabrication strategy has produced optical microring-resonator-based thermal detectors. The detectors are based on the thermo-optic effect and are thermally isolated from a silicon wafer substrate so as to maximize the temperature excursion for a given amount of incident radiation and minimize the impact of thermal phonon noise. The combination of high-Q, thermal isolation, and lack of Johnson noise offers thermal microphotonic detectors the potential to achieve significantly greater room temperature sensitivity than standard bolometric techniques. Several batch fabrication strategies were investigated for producing thermal microphotonic detectors using waveguide materials such as LPCVD Silicon Nitride (Si_3N_4) on Oxide and Silicon on Insulator (SOI). Fabrication challenges and loss reduction strategies will be presented along with some initial infrared detection results.

Keywords: Waveguide, integrated optics devices, resonators, optical loss, silicon nitride, infrared sensing

1. INTRODUCTION

The high quality factors (Q) that have been demonstrated in optical microring resonators have enabled the design and demonstration of highly sensitive microring-resonator-based sensors. Examples include chemical, biological, nuclear, inertial, and in this paper, thermal sensors[1-4]. The thermal sensor design described herein consists of a waveguide resonant microring structure, which is evanescently coupled to a bus waveguide, and thermally insulated from the substrate. The conceptual drawing shown in Figure 1a illustrates the major components of a thermal microphotonic detector element. The top absorber is connected to the microring resonator so as to transfer the thermal energy to the microring. Narrow tethers connect the ring to the thermally insulating support post, providing insulation between the substrate and the microring body. The same insulating material that supports the center post supports the bus waveguide. The insulating post and tethers serve two purposes: the thermal insulation (1) maximizes the temperature excursion in the microring, and (2) isolates the microring from the substrate thereby reducing the impact of thermal phonon noise caused by energy exchange between the microring and the substrate. The fundamental noise floor for thermal detection or the Noise Equivalent Power (NEP), has a spectral density represented in Equation 1,

$$NEP_{phonon} = \sqrt{4k_B G T} \tag{1}$$

where G is the thermal conductance to the substrate, k_B is the Boltzmann constant, and T is the temperature in Kelvin. The device is intended to function in the infrared and long-wave regions of the spectrum where photon detectors require either cryogenic cooling or do not exist. The absorbed thermal energy causes a temperature shift in the resonator and a shift in resonant wavelength, which is then detected in the bus waveguide signal. An example of how a resonance is shifted when incident radiation is detected can be seen in Figure 1b. Changes in transmission of an interrogating laser are then detected at the output of the bus waveguide with a photodiode detector. That is, when thermal energy is absorbed, it causes a shift in the resonant wavelength of the microring which is sensed as a change in the power level at the photodiode. Figure 1c shows an example of how a focal plane array could be designed. The scale factor, is given by

$$\frac{\Delta S}{S \cdot P_{abs}} = -\frac{Q}{G} \frac{d\lambda_0}{\lambda_0 dT} \tag{2}$$

where S is the signal, P_{abs}, is the absorbed power, λ_0 is the resonant wavelength, G is the thermal conductance to the substrate, Q is the quality factor, and $\dfrac{d\lambda_0}{\lambda_0 dT}$ is the thermo-optic coefficient for a resonator. While the scale-factor is important for high sensitivity, it is important to note that the fundamental noise performance is not determined by the scale factor or the resonator-Q, but rather by the phonon noise which has only two free parameters, the thermal conductance G, and the temperature T. Based on shot noise considerations, a relatively low-Q will still enable the fundamental noise limits to be reached. While very high-Q microsphere and micro-toroid-based devices have previously been demonstrated, the lack of an integrated coupling strategy precludes the development of sensor arrays required for applications such as thermal imaging. Thus, here, we only consider fabrication strategies with full wafer scale integration of the required optical components.

A detailed description of the motivation and detection strategy for a large array of ring elements can be found in a previous publication by Watts et al[3]. In short, a massive scale factor (> 1000X that of microbolometers), the lack of metal thermal paths (i.e. greater thermal isolation), and the elimination of Johnson noise together enable the possibility for much improved noise performance at room temperature.
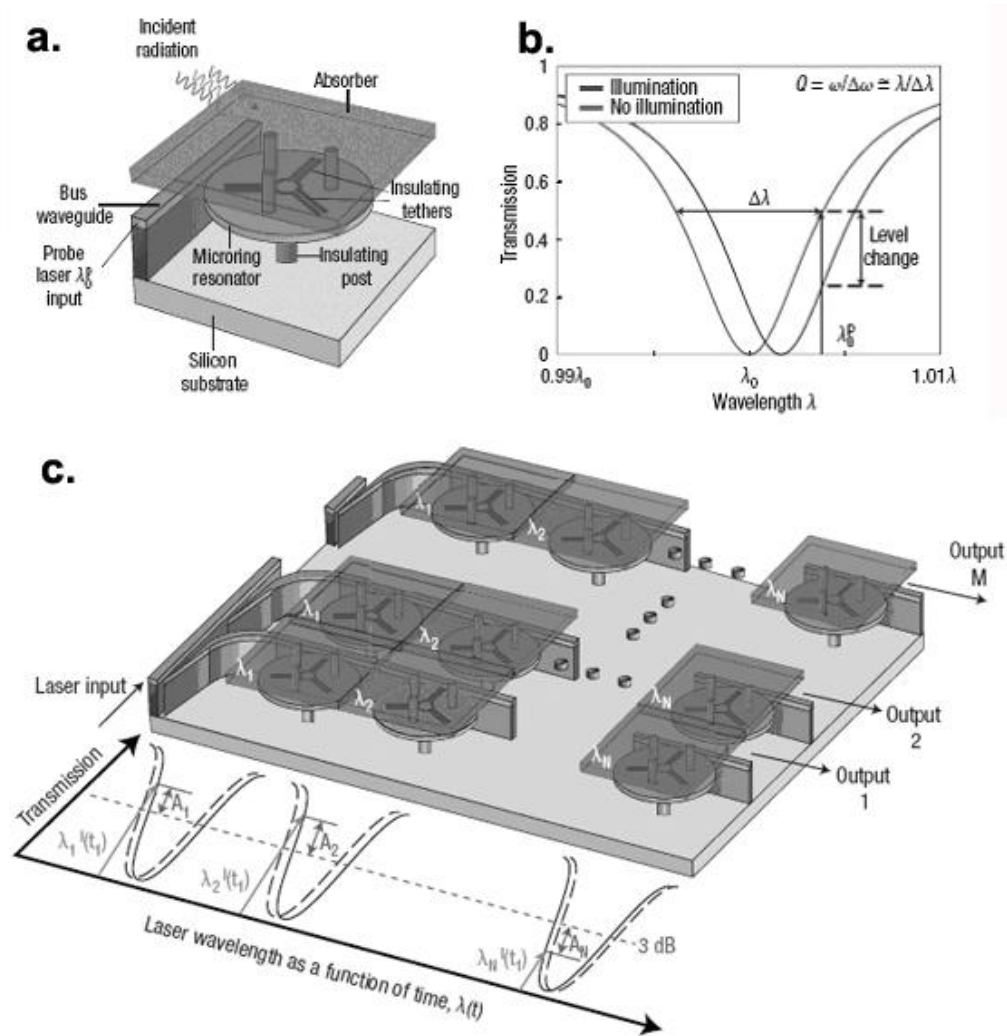

Figure 1. a) Schematic of a thermal microphotonic detector. The detector consists of a thermally isolated microphotonic resonator thermally coupled to an absorbing element and evanescently coupled to a bus waveguide. b) In its simplest form, the readout consists

of a probe laser at the 3-dB point of the resonance. On illumination, the temperature of the microresonator increases, shifting the resonant wavelength by means of the thermo–optic effect, and a change in transmission is detected. (Here, ω is the microring-resonator frequency, λ_0 is the resonant wavelength of the resonator with no illumination and λ_0^P is the probe wavelength.). c) Concept for a TM-FPA. The TM-FPA approach depicted uses a WDM-based readout technique to probe columns of sensors. The resonances can be probed by simply stepping the laser to the 3-dB point of the initial center wavelength of each column and reading out the amplitudes of transmission. This concept is just one possibility, and alternative approaches with greater linearity and dynamic range exist. [First published in [Nature Photonics, Volume 1, No. 11, 2007 November] Nature Publishing Group, a Division of Macmillan Publishers Limited]

2. DESIGN AND FABRICATION STRATEGIES

Thermal isolation is the foremost concern in the design of a room temperature microring based TM-FPA. Moreover; the fabrication processes, material system, and design must function well with each other in order to achieve success. Low loss silicon nitride waveguide technology developed at Sandia National Laboratories has been used to demonstrate high-Q microring resonators with Q's greater than 100,000.[4] The materials and processes required to create the low loss wave-guides are commonly found in standard integrated circuit fabrication facilities. High temperature processes are essential to achieving low loss in the silicon nitride technology. Process strategies must accommodate these high temperatures before diffusion sensitive materials are introduced. The silicon nitride waveguide core material is typically clad with silicon dioxide, a material with low thermal conductivity that can be used for the insulating post on the microring and bus waveguide support. Several strategies were evaluated for creating test devices and thermal modeling was performed prior to mask definition. Several material and geometry schemes were considered and two designs were selected for manufacture. The two material systems that were selected are 1) silicon nitride microring waveguide structure and 2) a single crystal silicon microring waveguide structure. Both strategies will be discussed in detail below.

2.1 Thermal modeling
The fundamental limit on sensitivity for a bolometer is the thermal noise resulting from the transfer of thermal energy between the substrate and the temperature sensing element (in this case the optical ring resonator). By decreasing the thermal conductivity between the ring resonator and the substrate, the thermal noise is reduced. Here we analyze two possible ring resonator bolometer designs for thermal energy flow between the ring resonators and the substrate. We also model the mechanical resonant frequency of the designs to evaluate any vibrational issues.

In both designs, the rings will be under vacuum. This essentially eliminates convective heat transfer and conduction through air to the substrate. This leaves conduction through the support structure and radiation as the only paths of heat transfer. Of these two heat transfer mechanisms, conduction dominates the heat transfer of the designs. We will therefore focus our analysis on conduction to estimate the heat transfer characteristics, and therefore sensitivity, of these designs. The material properties used in the models are given in Table 1.

Table 1 Material properties used in the finite element simulations.

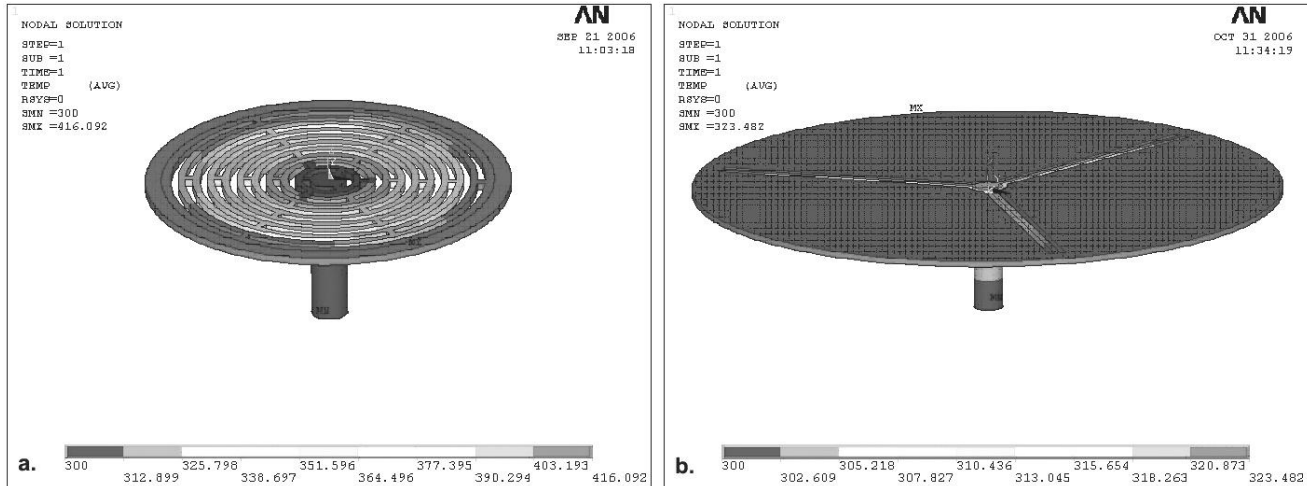|	Density (kg/m^3)	Specific Heat (J/kg·K)	Thermal Conductivity (W/m·K)	Elastic Modulus (GPa)	Poisson's Ratio
Silicon	2330	712	148	160	0.2
Silicon Oxide	2220	745	1.38	69	0.17
Silicon Nitride	2400	691	16	270	0.27

Figure 2 a) Temperature distribution resulting from a heat flux of 1×10^5 W/m^2 entering the top surface of the ring resonator. The supporting scaffold is constructed of silicon oxide. b) Temperature distribution resulting from a heat flux of 1×10^5 W/m^2 entering the top surface of the ring resonator. In this case the ring is the outer 0.45 μm of the disk. The supporting scaffold is constructed of silicon nitride in the plane of the ring. The post is silicon oxide.

2.2 Silicon oxide isolation scaffold

Conduction through the silicon oxide scaffold to the substrate was modeled by finite element analysis (FEA) with ANSYS. Figure 2a shows the temperature profile of the structure with a heat flux of 1×10^5 W/m^2 on the top surface of the ring. The ring has an outer radius of 5.0 μm and an inner radius of 4.55 μm, giving a total area of 1.35×10^{-11} m^2. The resultant heat flow from the ring to the substrate is 1.35 μW. The temperature difference experienced between the ring and the substrate for this heat flow is 116.1 K. The thermal conductance of this design is therefore 1.2e-8 W/K.

The supporting scaffold in this case is composed of the in-plane concentric rings with supports connecting the rings, and the post that extends down to the substrate. The in-plane support structure provides 90 - 95% of the thermal resistance in the structure. The lowest mechanical resonant frequency of this structure was found to be greater than 1 MHz. Because of this high resonant frequency, neither environmental acoustic vibrations nor thermally induced mechanical vibrations will likely disturb the sensing signal.

2.3 Silicon nitride absorber/scaffold

The post for this structure is identical to that of the silicon oxide model to allow comparison between the results. Since silicon nitride has a lower index than silicon, the optical ring resonator requires a larger diameter. The diameter of the ring in the simulation is 20 μm. The thermal flux that was applied to the ring in this case is the same as that applied in the silicon oxide case (1×10^5 W/m^2). Figure 2b shows the temperature profile of the structure (note that the gray contours are scaled differently than for the silicon oxide case). The temperature difference observed between the ring and the substrate is 23.5 K. This results in a thermal conductance of 1.17×10^{-7} W/K.

For this structure the silicon oxide post provides roughly 30% of the thermal isolation. The silicon nitride supporting structures can be folded to extend the thermal path length and therefore decrease the thermal conductance. This would result in slightly less efficient absorption and utilization of the incoming IR radiation. There is likely some optimal thermal path length that would maximize the sensitivity of the bolometer cell given this constraint. In addition, thin film values for the thermal conductivity of silicon nitride have been reported to be significantly lower than the bulk value used in this analysis[5]. Therefore, these results are conservative.

The lowest mechanical resonant frequency of this structure is 420 kHz. This is much less than the silicon oxide structure resonant frequency but is still very high. Environmental or thermally induced mechanical vibrations should not be a significant factor in the performance of the structure.

Further analysis is also required to determine the thermal capacitance of the structures which, when combined with the thermal conductance, will provide the thermal time constant of the structure. This time constant will effectively limit the bandwidth of the thermo-optic focal plane array.

2.4 Silicon nitride fabrication example
The design incorporating a silicon nitride microring with silicon nitride tethers and a silicon dioxide insulating post was selected as one of the first demonstration designs to be fabricated. The configuration shown in Figure 3a shows an idealized model of the designed geometry and Figure 3b, a scanning electron microscope (SEM) image of the a fabricated device. Both stoichiometric silicon nitride and low stress nitride (LSN), (i.e. silicon rich silicon nitride), waveguide materials were investigated in the initial fabrication attempts. The stoichiometric silicon nitride material proved to be a better choice than the LSN material due to limitations in the photo resist (PR) thickness and the reactive ion etch (RIE) capability. LSN was also shown in a previous study to have higher optical loss. The fine details required in the fabrication of these devices required the use of an ASML scanner stepper with a minimum resolution capability of 150 nm, and maximum PR thickness of 1.3 um.

The fabrication process for the thermally isolated silicon nitride microrings is illustrated in Figure 4a-e. In order for the ring element to be of use, many ring devices must be processed in an array with very high uniformity. The first fabrication attempt was successful in creating the desired geometry by using PR as the masking material for the undercut etch mask shown in Figure 4d, but the undercut was non-uniform. In some areas the isotropic oxide undercut step ran along the interface of the PR and undercut the PR at the same time as the microring. To remedy the problem the PR mask was replaced with a hard mask made of polysilicon, which produced very uniform and repeatable structures. A uniform array of completed devices can be seen in Figure 5.
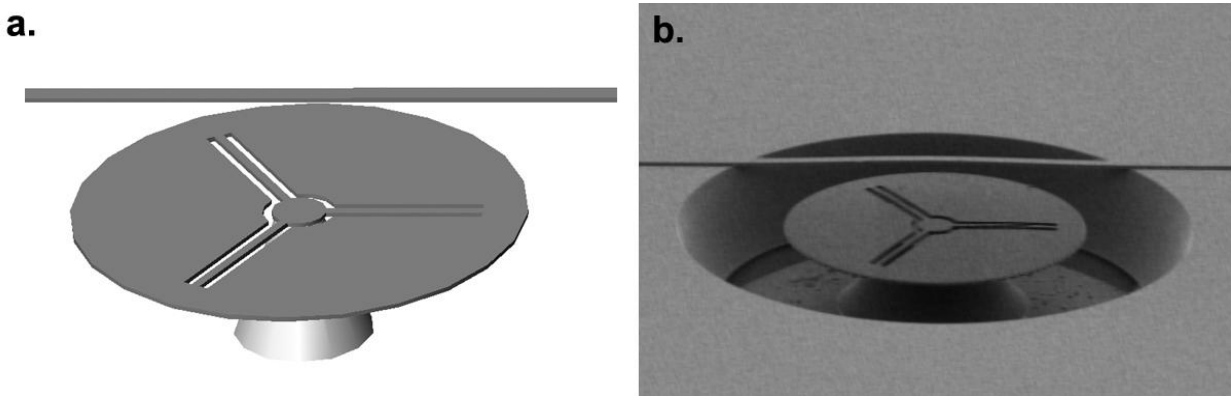

Figure 3. a) 3D model of the silicon nitride microring design. b) Fabricated silicon nitride microring.
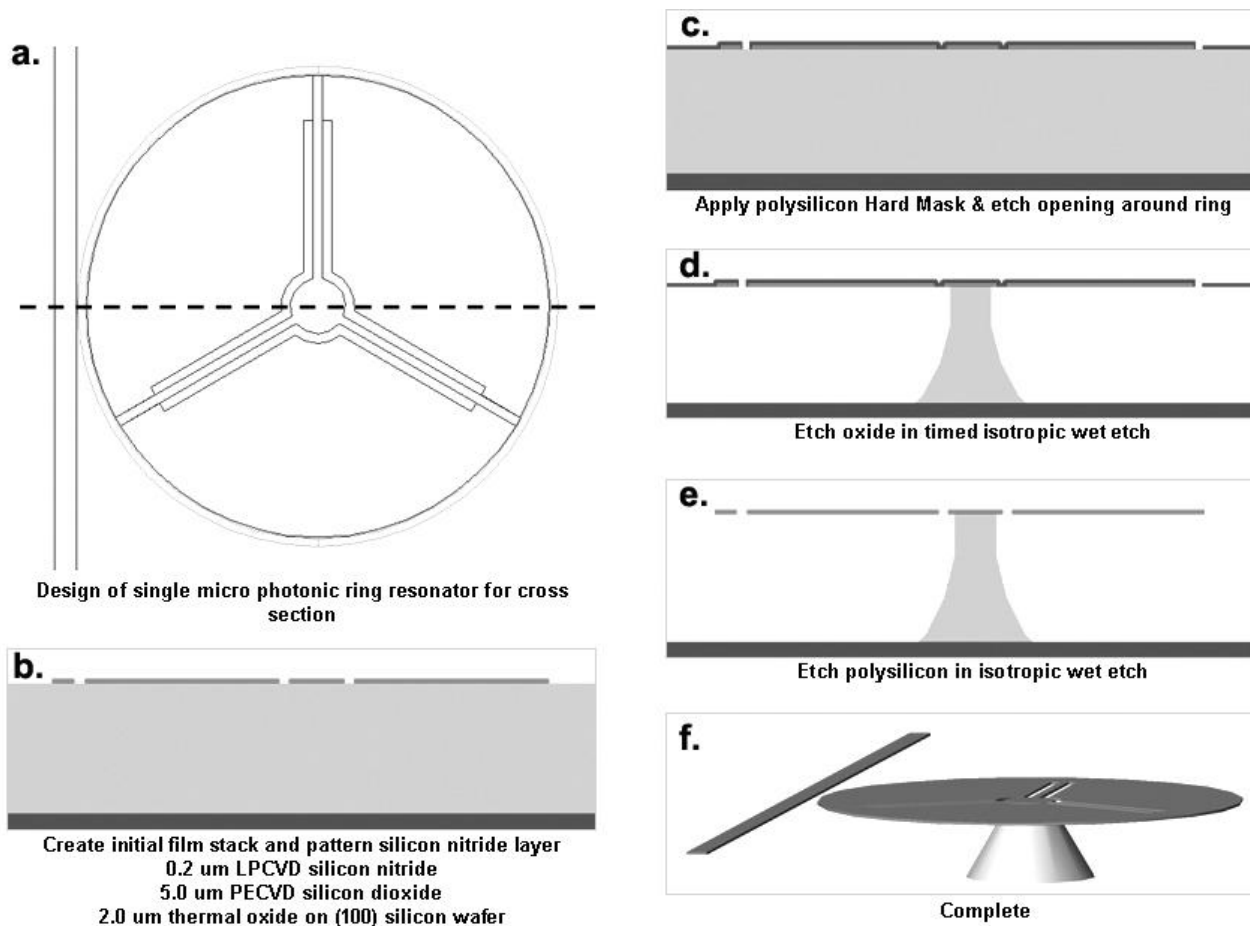
Figure 4. Process steps required in fabricating the silicon nitride microring TM-FPA sensor. Two dimensional (2D) renderings were generated with the Sandia 2D Process Visualizer, Version 2.35, generated from the photolithography mask design file drawn in AutoCAD ™.
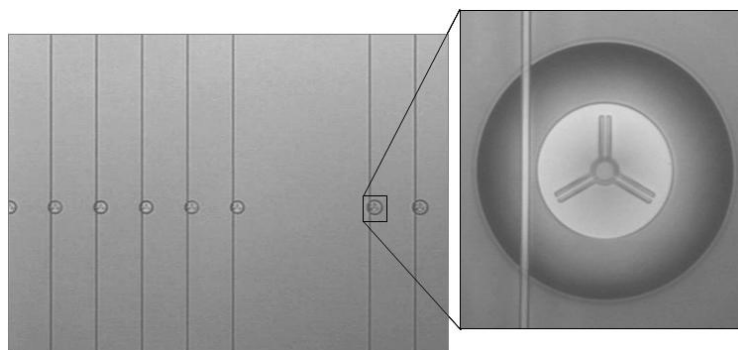

Figure 5. Array of uniform micro rings demonstrating uniform undercut etch.

2.5 Silicon on insulator (SOI) fabrication example

The single crystal silicon microring waveguides were created from SOI wafers with a 0.5 µm device layer with a 3.0 µm buried oxide (BOX) layer that were purchased from Soitec Inc. Figure 6a shows the 3D model of the design along with an SEM image in Figure 6b of a fabricated silicon nitride device using the design for the silicon ring. The tethers that support the microring to the center post are 50 nm wide. The fabrication of the silicon ring is similar to the silicon nitride process except certain materials have been substituted and a final oxidation step was employed to both smooth the waveguides and oxidize the tethers completely into silicon dioxide to form a high-quality insulating tether material

between the ring and the center post. The design is different from the nitride structure in that the tethers are now more complex in geometry and the geometries are much smaller. Details of the process flow are illustrated in Figure 7. The two dimensional (2D) renderings were generated with the Sandia 2D Process Visualizer, Version 2.35, generated from the photolithography mask design file drawn in AutoCAD ™.
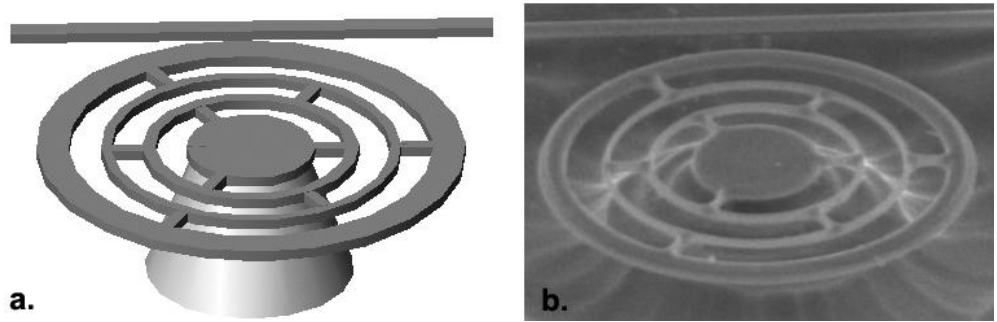

Figure 6. a) Idealized 3D model of Silicon on Insulator (SOI) microring design. b) fabricated microring.
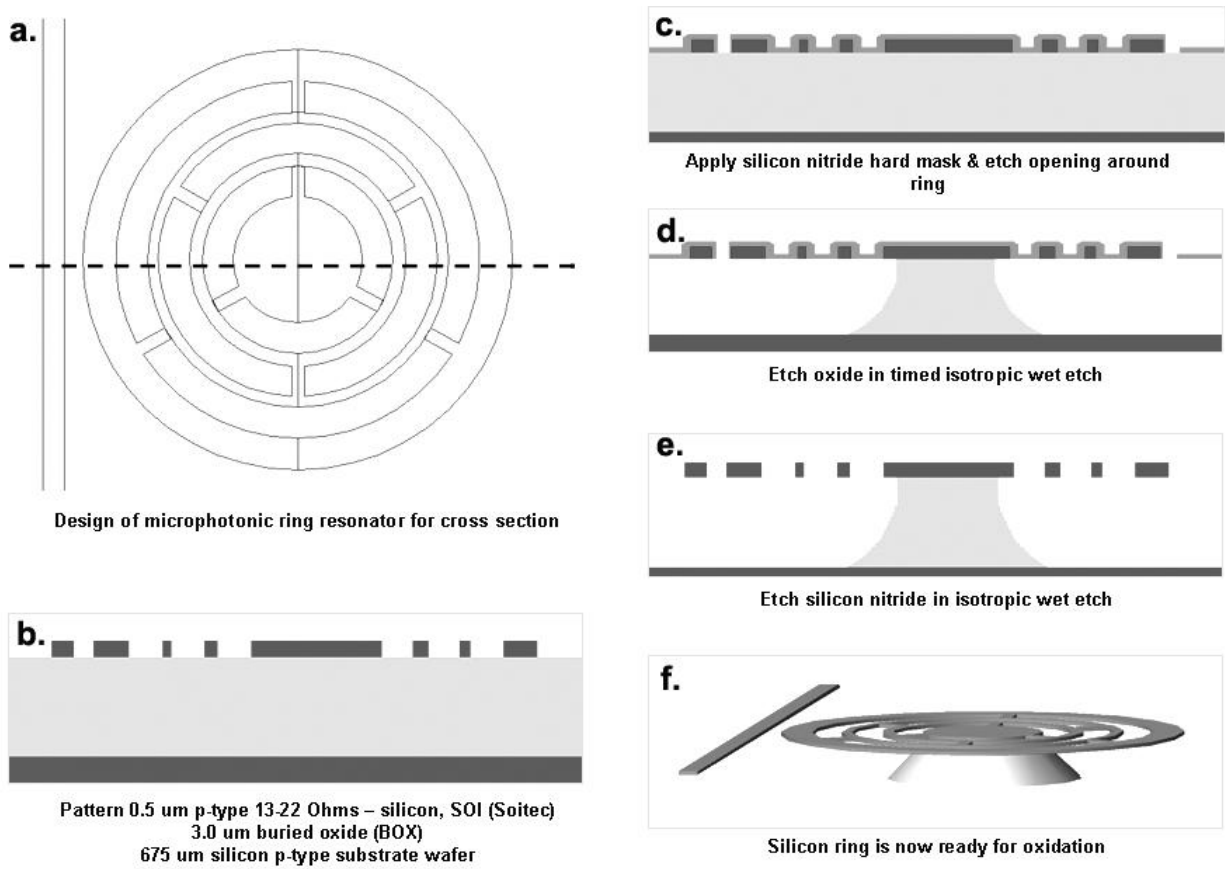

Figure 7. Process steps required in fabricating a silicon microring TM-FPA.

The fabrication of the silicon rings was performed by etching the pattern in the SOI silicon layer, applying a silicon nitride hard mask to the patterned structures, and patterning the outer ring opening for the wet isotropic undercut etch. The silicon ring undercut was similar in uniformity as in the silicon nitride case and the final suspended structure was oxidized in steam to cause the tethers to become a thermally insulating lattice of high quality silicon dioxide as can be

seen in Figure 8a. The silicon bus and microring waveguide were designed large enough to only partially oxidize and would remain encased in an oxide cladding. Images in Figure 8c and 8d show the fine nano structures left behind in the tether regions of the silicon rings after oxidation and stripping of the oxide in Hydrofluoric acid (HF). No silicon ring devices fabricated according to the design shown in Figure 7 survived the wet processing to remove the outer thermal oxide as indicated in Figure 8b. This indicates that the silicon in the tethers was completely oxidized as intended or that whatever silicon remained was so small it was broken in the wet processing.

Thermally grown silicon oxide develops a significant compressive residual stress. If unconstrained, as in the case of the undercut tethers, a linear growth of about 22% is expected. The deflection in the tethers shown in Figure 8a is a result of this expansion. The design of the tethers allowed for this deflection and it is clear that the structure behaved as intended and also supported the ring. Figure 8c, the oxidized tethers also supports the ring on the oxide post but some silicon remains un-oxidized. Figure 8d shows the remaining nano tethers after the HF strip process where the un-oxidized silicon is only 27 nm wide.
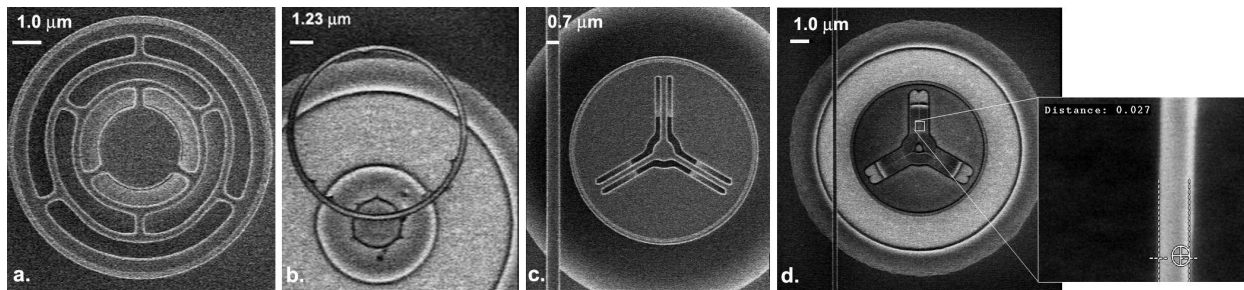

Figure 8. a) SEM image of an oxidized silicon ring with silicon dioxide in place. b) SEM image of an oxidized silicon ring with silicon dioxide stripped away in HF, indicating the silicon tethers were completely oxidized. c) SEM image of a silicon ring created with the design shown in Figure 4 with the silicon dioxide still in place. d) SEM images of the nanoscale tethers remaining after oxidation with the oxide stripped away in HF.
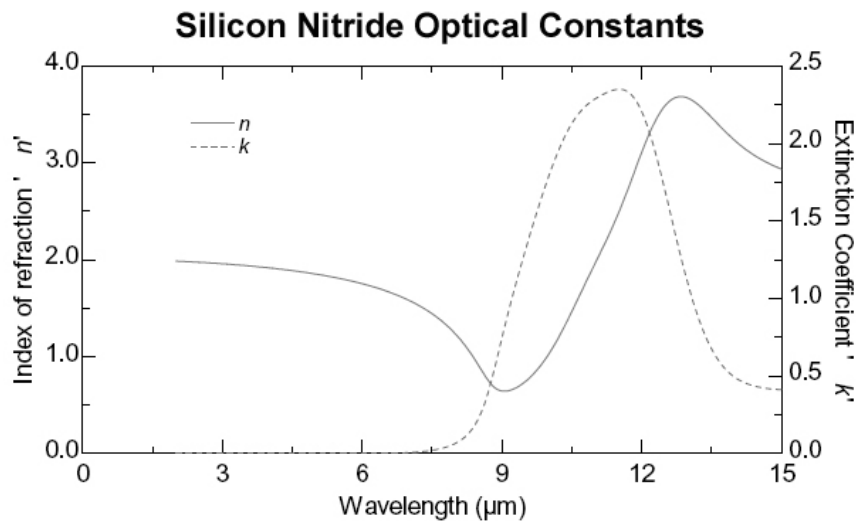

Figure 9. Plot of optical constants for silicon nitride material used in the microring showing good extinction at wavelengths between 9 and 13 µm. The data in graph was measured by J. A. Woollam Co., Inc. with a IR-VASE® ellipsometer.

2.6 Absorber strategy

The silicon nitride devices discussed in this work have a large surface area for absorbing incident radiation, however, this absorbing structure is not optimized. The silicon devices have no absorbing structure in the design. In this section we present work to support an independent absorber structure for absorbing radiation and transmitting thermal energy to the

microphotonic ring. Optical constants were measured for the silicon nitride material used in some of the designs. The plot in Figure 9 shows strong extinction at wavelengths between 9 and 13 µm, indicating that the silicon nitride ring material is a good candidate material for an absorber structure at those wavelengths. The results shown in figure 10 were generated with the use of a 10.6 µm CO_2 laser aimed directly at the silicon nitride microring surface in a proof of concept demonstration. The next generation devices to be fabricated will have a second silicon nitride layer suspended above the microring and attached to the outer portion of the ring with a nitride post as shown in Figure 1a. The fill factor for the top plate can be quite high as can be seen in the schematic drawing shown in Figure 1c.

3. EXPERIMENTAL TEST RESULTS

The test results for the silicon nitride ring results shown in Figure 10 show the response to incident radiation with a wavelength of 10.6 µm. The data was obtained by probing the 3-dB point of the resonance with a near-infrared laser (λ = 1.5 +m) and illuminating the microphotonic resonator with approximately 1 µW of power from a carbon dioxide laser. The set-up exploits the strong absorption of silicon nitride at wavelengths of λ = 9–13 µm and the transparency of silicon nitride to the near-infrared probe laser.
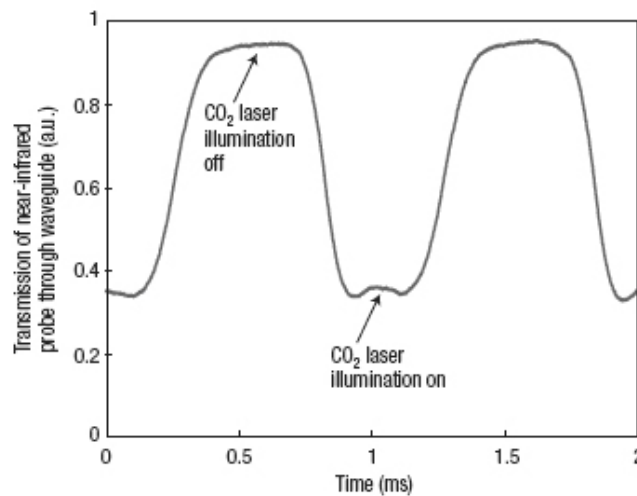

Figure 10. Response of the microphotonic thermal detector to an on–off modulated (that is, chopped) CO_2 laser signal at a wavelength of λ = 10.6 µm and with about 1 µW of incident power. The temperature change resulting from the silicon nitride microphotonic resonator absorbing the carbon dioxide laser light induces a change in the transmission of the near-infrared (λ = 1.5 µm) laser line probing the resonator. [First published in [Nature Photonics, Volume 1, No. 11, 2007 November] Nature Publishing Group, a Division of Macmillan Publishers Limited]

Experimental results for silicon ring structures were not possible due to the over oxidation of the silicon mentioned in section 2. The over oxidation of the bus and microring waveguides caused the evanescent coupling gap to be too large and therefore no critical coupling to the rings was possible. More work will be needed to demonstrate experimental results from the SOI fabrication strategy, but the high index of refraction of silicon makes it desirable for very small ring geometries allowing for the creation of small pixels and high resolution arrays. Interestingly, the over-oxidation and, subsequent failure of the silicon rings, highlights one of the more challenging parts of creating large arrays, specifically, the critical dimension (CD) control and the uniformity of the coupling gap. It is difficult to create consistency over an entire wafer surface in microelectronics processing at the level that will be necessary to scale up to a large array. The number of pixels possible in a single array may be limited by the resolution capability of the tool set being used to create them, where the critical coupling gap dimensions must be highly controlled and repeatable. The silicon nitride geometry with a larger coupling gap requirement is more amenable to the tool set that was used in this prototype fabrication cycle,

where the photolithography tool resolution capability is 150 nm. It is fortunate that the IC industry has found the need to drive feature sizes ever smaller with Extreme Ultra Violet (EUV) and Immersion Lithography targeting resolution capabilities below the 50 nm node size.

4. CONCLUSION

We set out to fabricate and demonstrate the elements necessary to create a room temperature Thermo Microphotonic Focal Plane Array (TM-FPA) with potential to rival current electron–hole pair photon detector technologies that require cryogenic cooling to image long wavelength radiation. Two strategies were attempted, one structure with silicon nitride waveguides and another structure with single crystal silicon waveguides, both using an isotropic undercut etch to create an insulating silicon dioxide support post under an evanescently coupled microring resonator. While both fabrication processes proved encouraging, the silicon nitride process was the most robust. We demonstrated uniform ring geometry in a line array, novel strategies for creating nano scale insulating tethers, and radiation detection at a wavelength of 10.6 μm at room temperature. Future work will include the addition of an absorber plate suspended above the microrings in a large array of imaging elements such as shown in Figure 1a, with the ultimate goal of demonstrating a fully functional room temperature microphotonic imager.

REFERENCES

1. Guo, J., Shaw, M. J., Vawter, G. A., Hadley, G. R., Esherick, P., and Sullivan, C. T., "High-Q microring resonator for biochemical sensors", *Integrated Optics: Devices, Materials, and Technologies IX*, Proceedings of SPIE, Vol. 5728, p. 83-92, March 2005.
2. Suzuki, K., Takiguchi, K., "Monolithically Integrated Resonator Microoptic Gyro On Silica Planar Lightwave Circuit", *J. of Lightwave Tech*., Vol. 18, p. 66-72, January 2000.
3. Watts, M. R., Shaw, M. J., Nielson, G. N., "Microphotonic thermal imaging" *Nature Photonics*, Vol. 1, p. 632-634, November 2007.
4. Shaw, M. J., Guo, J., Vawter, G. A., Habermehl, S., and Sullivan, C. T., "Fabrication techniques for low loss silicon nitride waveguides" *Micromachining Technology for Micro-Optics and Nano-Optics III,* Proceedings of SPIE, Vol. 5720, p. 109-118, 2005.
5. Radford, W., Murphy, D., Finch, A., Hay, K., Kennedy, A., Ray, M., Sayed, A., Wyles, J., Wyles, R., and Varesi, J., "Sensitivity improvements in uncooled microbolometer FPAs", *Infrared Technology and Applications XXV* Proceedings of SPIE, Vol. 3698, p. 119-130, July 1999.